[Communication] www.whxb.pku.edu.cn

$NiCo_2O_4$ 对 H_2O_2 在碱性溶液中电化学还原反应的催化行为

高胤义 曹殿学* 王贵领 尹翠蕾
(哈尔滨工程大学材料科学与化学工程学院, 哈尔滨 150001)

摘要: 利用溶胶-凝胶法合成了纳米 $NiCo_2O_4$, 并利用 X 射线衍射和透射电镜分析了其结构和表面形貌. 结果表明 $NiCo_2O_4$ 具有尖晶石结构, 其平均粒径约为 15 nm. 利用电势线性扫描和恒电势法测定了其对 H_2O_2 在碱性溶液中电化学还原反应的催化性能. 发现 $NiCo_2O_4$ 对 H_2O_2 电化学还原具有高的催化活性和稳定性, 在 H_2O_2 浓度低于 0.6 mol·L^{-1} 时, 其电化学还原反应主要通过直接还原途径进行. 以 $NiCo_2O_4$ 为阴极催化剂的 Al-H_2O_2 半燃料电池在室温下的开路电压达 1.6 V; 在 1.0 mol·L^{-1} H_2O_2 溶液中, 峰值功率达 209 mW·cm^{-2}, 此时电流密度为 220 mA·cm^{-2}.

关键词: 钴酸镍; 过氧化氢; 电化学还原; 阴极催化剂; 金属半燃料电池
中图分类号: O646.5; O643

Catalytic Behavior of $NiCo_2O_4$ for H_2O_2 Electroreduction in Alkaline Medium

GAO Yin-Yi CAO Dian-Xue WANG Gui-Ling YIN Cui-Lei
(*College of Material Science and Chemical Engineering, Harbin Engineering University, Harbin 150001 P. R. China*)

Abstract: $NiCo_2O_4$ nanoparticles were synthesized using a sol-gel method. Their structures and morphologies were characterized using X-ray diffraction (XRD) and transmission electron microscopy (TEM). Results indicate that $NiCo_2O_4$ has a spinel structure and an average diameter of around 15 nm. The catalytic behavior of $NiCo_2O_4$ for H_2O_2 electroreduction in alkaline media was investigated by linear potential sweep and chronoamperometry. $NiCo_2O_4$ shows considerable activity and stability for the electrocatalytic reduction of H_2O_2. The electroreduction occurs mainly *via* a direct pathway at H_2O_2 concentrations lower than 0.6 mol·L^{-1}. An Al-H_2O_2 semi-fuel cell was constructed using $NiCo_2O_4$ as the cathode catalyst. The cell displays an open circuit voltage of 1.6 V and a peak power density of 209 mW·cm^{-2} at 220 mA·cm^{-2} running on 1.0 mol·L^{-1} H_2O_2 at ambient temperature.

Key Words: Nickel cobaltite; Hydrogen peroxide; Electrochemical reduction; Cathode catalyst; Metal semi-fuel cell

Fuel cells for use in air-free environments, such as in space or underwater, require liquid or constringent O_2 as cathode oxidant. The bulky tank for carrying O_2 significantly reduces the energy density and safety standard of fuel cell systems. Since high energy density and safety are critical for fuel cells as space or underwater power sources, alternative oxidants other than O_2 have been investigated, such as H_2O_2. In recent years, several types of fuel cells using H_2O_2 as oxidant have been reported, including direct methanol-hydrogen peroxide fuel cells[1–3], direct borohydride-hydrogen peroxide fuel cells[4–6], and metal-hydrogen peroxide

Received: September 9, 2009; Revised: October 16, 2009; Published on Web: November 9, 2009.
*Corresponding author. Email: caodianxue@hrbeu.edu.cn; Tel/Fax: +86-451-82589036.
The project was supported by the National Natural Science Foundation of China (20973048), Key Laboratory of Superlight Material and Surface Technology of Ministry of Education of China, Heilongjiang Postdoc Foundation, China (LBH-Q06091), and Fund of Harbin Engineering University, China (HEUFT07030, HEUFT07051).
国家自然科学基金(20973048), 中国教育部超轻材料与表面技术重点实验室开放基金, 中国黑龙江省博士后基金(LBH-Q06091)和中国哈尔滨工程大学基础研究基金(HEUFT07030, HEUFT07051)的资助

semi fuel cells[7–17].

H_2O_2 as fuel cell oxidant has many advantages: (1) H_2O_2 is a powerful oxidant and can be converted into hydroxyl radicals with a reactivity second only to fluorine[5]; (2) the single O—O bond energy of H_2O_2 (51 kJ·mol^{-1}) is much lower than the double O═O bond energy of O_2 (498 kJ·mol^{-1}). The exchange current density of H_2O_2 reduction is around 3–6 order higher than that of O_2 reduction[18,19], so fuel cells using H_2O_2 as oxidant tend to provide higher performance than that using O_2 as oxidant; (3) H_2O_2 is liquid and its handling, storage, and delivery to a fuel cell are easy, which make the fuel cell system more compact and convenient; (4) the electroreduction reaction of liquid H_2O_2 occurs in a solid/liquid two-phase reaction zone of the cathode, while O_2 electroreduction requires a solid/liquid/gas three-phase region (gas diffusion electrode). The two-phase reaction zone is more readily realizable and easier to maintain during fuel cell operation than the three-phase region.

The performance of H_2O_2 cathode significantly depends on the nature of cathode catalysts. Several types of H_2O_2 electroreduction electrocatalysts have been investigated, including noble metals (Pt, Pd, Ir, Au, Ag, and a combination of these metals)[4–8,11,20], macrocycle complexes of transition metals (Fe- and Co-porphyrin, Cu-triazine complexes)[21–23], and other types such as $PbSO_4$ and Co_3O_4[17,23]. Among these types of electrocatalysts, the most active and stable one is the noble metal type. However, noble metals, besides expensive, also catalyze the chemical decomposition of H_2O_2 to O_2. The evolved O_2, if not further electroreduced, will contribute little usable electrical energy, and therefore robs the system of energy density. Therefore, seeking electrocatalysts with low cost and less active for H_2O_2 decomposition is necessary. Our previous study[17] demonstrates that Co_3O_4 nanoparticles have good activity and stability for electrocatalytic reduction of H_2O_2 in alkaline solution.

$NiCo_2O_4$ has been known to be an active and stable bifunctional catalyst for O_2 evolution and reduction in alkaline media[24–27]. Structure analysis has shown the existence of Ni^{2+}, Ni^{3+}, Co^{2+}, and Co^{3+} in this compound[28,29]. The redox couples of Ni^{2+}/Ni^{3+} and Co^{2+}/Co^{3+} might be responsible for the catalytic activity of $NiCo_2O_4$ for oxygen reduction and evolution. H_2O_2 radicals has been proposed to be the intermediate of oxygen electroreduction on $NiCo_2O_4$[27], which suggests that $NiCo_2O_4$ might possess activity for direct electroreduction of H_2O_2.

In this paper, nano-sized $NiCo_2O_4$ particles were prepared and their electrocatalytic activity and stability for H_2O_2 electroreduction were investigated. The performance of an Al-H_2O_2 semifuel cell using $NiCo_2O_4$ as cathode catalyst was evaluated. This study opens up a possibility for the development of a low cost H_2O_2 electroreduction catalyst.

1 Experimental

1.1 Synthesis and characterization of $NiCo_2O_4$

$NiCo_2O_4$ powder was synthesized by a sol-gel method. $Ni(NO_3)_2 \cdot 6H_2O$ (>99.0%), $Co(NO_3)_2 \cdot 6H_2O$ (>99.0%) and NH_4HCO_3 (NH_4: 21.0%–22.0%) were used as source materials without further purification. Equal volumes of 1.0 mol·L^{-1} cobalt nitrate and 0.5 mol·L^{-1} nickel nitrate aqueous solution were mixed thoroughly. 3.3 mol·L^{-1} NH_4HCO_3 solution was then added dropwise to the above mixture at room temperature under constant stirring. The molar ratio of $Ni(NO_3)_2$:$Co(NO_3)_2$:NH_4HCO_3 was 1:2:6.6. The resulting precipitate was separated from the solution by vacuum filtration, washed thoroughly with ultrapure water, and then dissolved in excess propionic acid (analytical grade, 150 mL per 100 g precipitate). The solution was heated at 140 ℃ to remove most of the excess water and propionic acid until a violet gel was formed. The gel was further heated at 180 ℃ in a stove under atmosphere for 24 h. After cooling to room temperature, the dry gel was finely ground and calcined at 300 ℃ in air for 3 h.

The phases and average particle size of the resulting powder were determined using an X-ray diffractometer (XRD, Rigaku TTR III, Japan) with Cu K_α radiation (λ=0.1514178 nm). The diffractograms were obtained in a scan range of 2θ from 10° to 80° with a step width of 0.01° and a scan rate of 5 (°)·min^{-1}. The morphology of the particles was examined using a transmission electron microscope (TEM, FEI Tecnai G2 S-Twin, Philips, Holland) equipped with an energy-dispersive X-ray spectrometer (EDX). Samples were dispersed in anhydrous ethanol and loaded on carbon-coated copper grids.

1.2 Preparation of $NiCo_2O_4$ electrode

To prepare $NiCo_2O_4$ electrode, $NiCo_2O_4$ powder and carbon black (Vulcan XC-72, Cabot Corporation, USA) were dispersed in anhydrous ethanol and sonicated for 15 min to obtain a suspension, to which a PTEF emulsion(40%, Jiangsu Huayuan H-Power Tech. Co., Ltd., China) was added. The mixture was sonicated for another 15 min and then heated at 80 ℃ in a water bath until a thick paste was formed. The paste was applied to a nickel foam current collector (Changsha Lyrun New Material Co. Ltd., China). The nickel foam containing the paste was then heated at 110 ℃ for 5 h. The dry weight ratio of $NiCo_2O_4$:carbon black:PTEF was 7:3:1. The obtained $NiCo_2O_4$/C/Ni-foam electrodes were used for both tests in the electrochemical cell as the working electrode and in the fuel cell as the cathode.

1.3 Electrochemical measurements

The electrochemical measurements were performed in a standard three-electrode electrochemical cell at room temperature using a 3.0 mol·L^{-1} NaOH (analytical grade) as the electrolyte solution. A glassy carbon rod behind a D-porosity glass frit was employed as the counter electrode and a saturated Ag/AgCl, KCl electrode served as the reference. The $NiCo_2O_4$/C/Ni-foam working electrode has a dimension of 10 mm×10 mm×0.5 mm (length×width×thickness) with a $NiCo_2O_4$ loading of around 15 mg·cm^{-2}. The cyclic voltammograms and chronoamperometry curves were recorded using a computerized VMP3/Z potentiostat (Princeton Applied Research, USA) controlled by EC-lab software. The reported currents were normalized to the geometrical area of the electrode. All solutions were made with Milli-Q water (18 M ·cm). All potentials were referred to the saturated Ag/

AgCl, KCl reference electrode unless specified.

1.4 Al-H_2O_2 semi-fuel cell tests

The performance of $NiCo_2O_4$ as cathode catalyst of the Al-H_2O_2 semi-fuel cell was examined using a home-made flow through test cell made of Plexiglas. The aluminum alloy anode (LF6, Northeast Light Alloy Co., Ltd.) and the $NiCo_2O_4$/C/Ni-foam cathode possessed the same geometrical area of 4.0 cm^2 (20 mm×20 mm). Nafion-115 (DuPont, USA) membrane was used to separate the anode and the cathode compartments. The anolyte (3.0 $mol \cdot L^{-1}$ NaOH) and the catholyte (3.0 $mol \cdot L^{-1}$ NaOH+ $x mol \cdot L^{-1}$ H_2O_2) were pumped into the bottom of the anode and the cathode compartments at a flow rate of 100 $mL \cdot min^{-1}$, respectively, and exited at the top of the compartments. The discharge performance of the Al-H_2O_2 semi-fuel cell was measured at ambient temperature using a computer-controlled E-load system (Arbin, USA).

2 Results and discussion

2.1 Characterization of $NiCo_2O_4$

A typical XRD profile of the synthesized $NiCo_2O_4$ powder calcined at 300 ℃ is shown in Fig.1, in which the standard powder XRD pattern of spinel $NiCo_2O_4$ from a JCPDS card 000-020-0781 (vertical lines) is included for comparison. Clearly, the pattern of our synthesized sample matches well with the standard XRD pattern of $NiCo_2O_4$, and only peaks due to the reflections of $NiCo_2O_4$ are visible. The cubic cell parameter is calculated to be a=0.812 nm, which corresponds with a=0.811 nm given by the JCPDS 000-020-0781 file. These results demonstrate that the synthesized sample is pure $NiCo_2O_4$ with a spinel structure. The calcination temperature is critical and should be controlled within the range of 250–350 ℃. Calcination at temperatures above 400 ℃ results in the decomposition of $NiCo_2O_4$ to NiO and Co_3O_4. Samples calcined below 250 ℃ exhibit an amorphous state. The broad XRD lines indicate the nano-crystalline nature of the material. The crystallite sizes are estimated using Scherrer′s relationship[30], $d=K\lambda/(B\cos\theta)$, where d is the average diameter in nm, K is the shape factor, B is the half width of the [440] peak, λ is the wavelength of X-rays (0.1514178 nm) and θ is Bragg′s diffraction angle. The estimated average crystallite size is 15 nm.

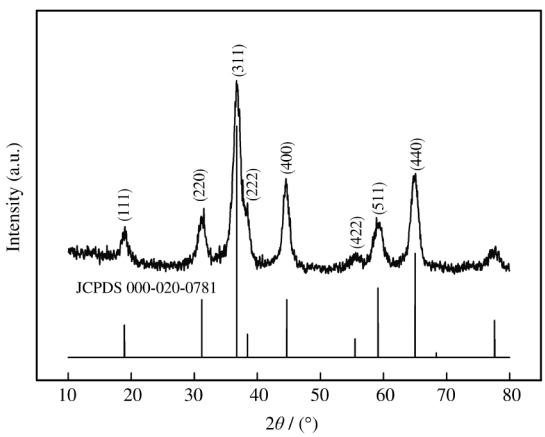

Fig.1 XRD pattern of $NiCo_2O_4$

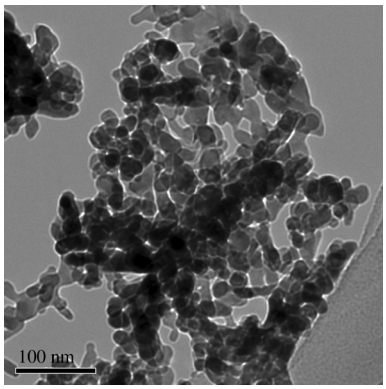

Fig.2 TEM image of $NiCo_2O_4$

TEM image of $NiCo_2O_4$ powder (Fig.2) confirms that the diameter of the individual $NiCo_2O_4$ particles is around 10–20 nm. The particles are roughly in spherical shape and agglomerate together. The EDX analysis indicates that the molar ratio of Ni to Co is 9.5:18.8, which agrees well with the stoichiometric ratio of Ni to Co in $NiCo_2O_4$.

2.2 Electroreduction of hydrogen peroxide on $NiCo_2O_4$ electrode

Fig.3 shows the current-potential polarization curves for the electroreduction of H_2O_2 with various concentrations on $NiCo_2O_4$/C/Ni-foam electrode. The onset potential for H_2O_2 electroreduction is around −0.16 V. Cathodic currents increase with the increase of H_2O_2 concentration. The current density is higher than that obtained on the Co_3O_4 electrode as we reported previously[17]. For example, a current density of 160 $mA \cdot cm^{-2}$ is achieved on the $NiCo_2O_4$ electrode, but only 120 $mA \cdot cm^{-2}$ is obtained on the Co_3O_4 electrode at −0.4 V for 0.6 $mol \cdot L^{-1}$ H_2O_2. It should be noted that even though high current density can be achieved at high H_2O_2 concentration, the chemical decomposition of H_2O_2 to O_2 becomes more significant at high H_2O_2 concentration. Interestingly, electrochemical current oscillation during H_2O_2 reduction on the $NiCo_2O_4$ electrode in 1.2 $mol \cdot L^{-1}$ H_2O_2 is observed within the potential range from −0.57 to −0.69 V. Similar phenomena have been reported for H_2O_2 reduction on metal (Pt, Au, and Ag) and semiconductor ($CuFeS_4$, $CuInSe_2$, and GaAs) electrodes in acidic, neutral, and basic medium[31,32]. We also measured the cur-

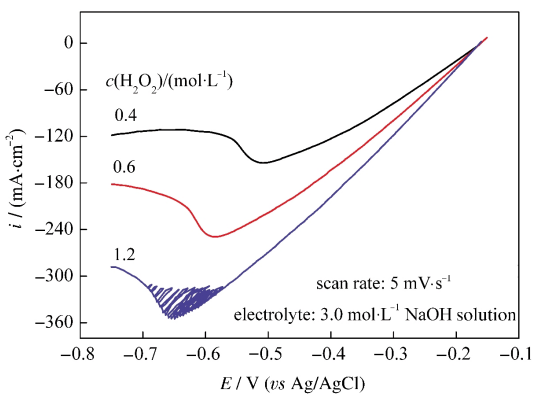

Fig.3 Current density (i)-potential (E) curves for H_2O_2 electroreduction on $NiCo_2O_4$ electrode

rent density–potential curve of C/Ni-foam electrode ($NiCo_2O_4$-free) in 3.0 mol·L^{-1} NaOH containing 0.6 mol·L^{-1} H_2O_2 and found the cathodic current density is less than about 1.5 mA·cm^{-2}, which is remarkably lower than that measured on $NiCo_2O_4$/C/Ni-foam electrode. This confirms the existence of the electrocatalytic activity of $NiCo_2O_4$ for H_2O_2 reduction.

The H_2O_2 cathode reaction can occur *via* a direct 2e$^-$ pathway or an indirect 4e$^-$ pathway. In the indirect mode, H_2O_2 first decomposes to O_2, which was then electro-reduced, so H_2O_2 simply serves as an O_2 carrier. In the direct mode, H_2O_2 is delivered to the cathode and directly reduced electrochemically ($H_2O_2+2e^- \rightarrow 2OH^-$). Clearly, the direct pathway is preferable because: (1) the direct electroreduction of H_2O_2 is a 2e$^-$ process and hence has a lower activation energy than the electroreduction of O_2 (4e$^-$ process); (2) the theoretical potential for the direct reduction of H_2O_2 (0.878 V) is higher than that for O_2 reduction (0.401 V) in a basic medium, so the direct reduction of H_2O_2 produces a larger cell voltage. We indeed noted the occurrence of chemical decomposition of H_2O_2 on $NiCo_2O_4$, particularly at H_2O_2 concentration higher than 0.6 mol·L^{-1}. Considering $NiCo_2O_4$ is able to catalyze O_2 electroreduction in alkaline medium[33–35], there is possible that the H_2O_2 electroreduction may go through the indirect pathway. In order to investigate *via* which pathway H_2O_2 reduction over $NiCo_2O_4$ proceeds, the cyclic voltammogram of $NiCo_2O_4$ is first taken in a blank 3.0 mol·L^{-1} NaOH solution (Fig.4, dot line), and then in an O_2-saturated 3.0 mol·L^{-1} NaOH solution (Fig.4, solid line). Clearly, an O_2 reduction peak is observed with the peak current density of 4.5 mA·cm^{-2} at –0.29 V. This current density, however, is nearly 6.3% of that for H_2O_2 reduction (71 mA·cm^{-2} for 0.4 mol·L^{-1} H_2O_2, Fig.3). So it can be concluded that H_2O_2 reduction on $NiCo_2O_4$ mainly proceeds through the direct 2e$^-$ pathway. The cyclic voltammogram of $NiCo_2O_4$ recorded in blank NaOH solution displays significant lower cathodic current densities than that taken in H_2O_2-containing NaOH solution. This result confirms that the cathodic currents are from the electroreduction of H_2O_2 and demonstrates the catalytic activity of $NiCo_2O_4$ for H_2O_2 electroreduction.

Fig.5 shows the current density–time curves for H_2O_2 electroreduction in 3.0 mol·L^{-1} NaOH+0.6 mol·L^{-1} H_2O_2 solution over $NiCo_2O_4$ electrode at various constant potentials. At –0.2 and

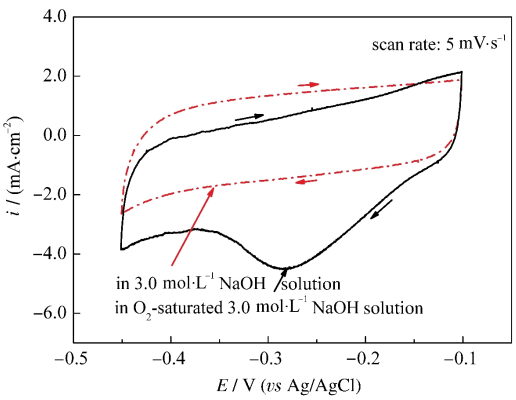

Fig.4 Cyclic voltammograms of $NiCo_2O_4$ electrode

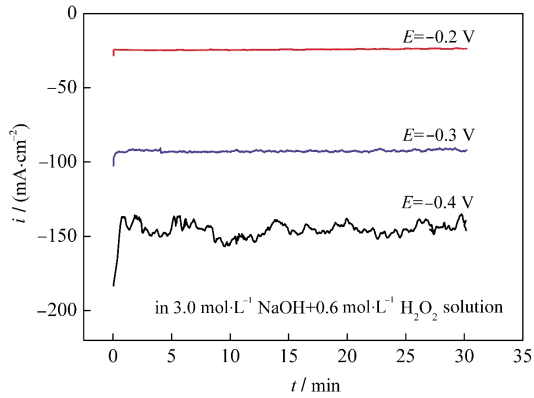

Fig.5 Chronoamperometric curves for H_2O_2 electroreduction at different potentials

–0.3 V, current densitions rapidly reach the steady-state and remain constant within a 30-minute test period, indicating $NiCo_2O_4$ being stable for H_2O_2 reduction. At –0.4 V, current densities irregularly fluctuate with the maximum amplitude of around 20 mA·cm^{-2}, but overall display no decrease. This behavior might result from the depletion of H_2O_2 near the $NiCo_2O_4$ surface and/or the current oscillation phenomena. The current densities are higher than previously reported on Co_3O_4 electrode[17], indicating that $NiCo_2O_4$ is more active than Co_3O_4.

2.3 Al-H_2O_2 semi-fuel cell test

In order to evaluate the performance of $NiCo_2O_4$ as the cathode catalyst for fuel cells using H_2O_2 as oxidant, an Al-H_2O_2 single semi-fuel cell was constructed to serve as a model fuel cell. Fig.6 shows the plots of cell voltage and power density *versus* current density at ambient temperature with varying concentrations of H_2O_2 solution feeding to the cathode. The cell has an open circuit voltage of 1.6 V. At current density below about 100 mA·cm^{-2}, the cell voltage decays linearly with the increase of current density and is independent of H_2O_2 concentration. At current densities higher than 100 mA·cm^{-2}, the cell performance depends on H_2O_2 concentration. A maximum peak power density of 209 mW·cm^{-2} at 220 mA·cm^{-2} was achieved when the cell operating on 1.0 mol·L^{-1} H_2O_2. Further increase of H_2O_2 conce-

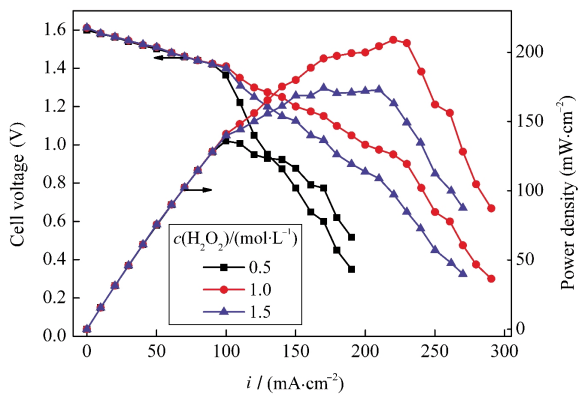

Fig.6 Plots of cell voltage and power density *versus* current density of the Al-H_2O_2 single semi-fuel cell with different concentrations of H_2O_2

anolyte: 3.0 mol·L^{-1} NaOH solution, catholyte: 3.0 mol·L^{-1} NaOH+H_2O_2 solution

ntration to 1.5 mol·L^{-1} reduces the cell performance. This is likely due to the severe decomposition of H_2O_2 as indicated by the generation of large numbers of O_2 gas bubbles on the cathode. The formation of O_2 bubbles reduces the effective electrode area for H_2O_2 reduction and affects diffusion of H_2O_2 to the $NiCo_2O_4$ surface.

It should be pointed out that the Al-H_2O_2 semi-fuel cell presented in this work is only for the demonstration of the feasibility of $NiCo_2O_4$ as a cathode catalyst for fuel cells using H_2O_2 as oxidant. The cell configuration, cathode structure and operation parameters, such as temperature and flow rate, are not optimized. The cell performance can be enhanced, for example, by reducing *IR* drop and improving cathode structure to allow better mass transport of H_2O_2. Notably, $NiCo_2O_4$ can also be used in other fuel cells using H_2O_2 as oxidant, such as direct alkaline $NaBH_4$-H_2O_2 fuel cells.

3 Conclusions

Spinel structure nano-sized $NiCo_2O_4$ particles are synthesized and tested as electrocatalyst for H_2O_2 reduction in alkaline medium. $NiCo_2O_4$ exhibits higher electrocatalytic activity than Co_3O_4 and has good stability in alkaline electrolyte. The electroreduction occurs primarily *via* the direct pathway at low H_2O_2 concentration. Chemical decomposition becomes severe at high H_2O_2 concentration. An Al-H_2O_2 semi-fuel cell constructed using $NiCo_2O_4$ as cathode catalyst displays an open circuit voltage of 1.6 V and a peak power density of 209 mW·cm^{-2} at 220 mA·cm^{-2} running in 1.0 mol·L^{-1} H_2O_2 solution at ambient temperature. This study demonstrates that $NiCo_2O_4$ is a promising low cost cathode catalyst for fuel cells using H_2O_2 as oxidant.

References

1 Prater, D. N.; Rusek, J. J. *Appl. Energ.*, **2003, 74**: 135

2 Bewer, T.; Beckmann, T.; Dohle, H.; Mergel, J.; Stolten, D. *J. Power Sources*, **2004, 125**: 1

3 Sung, W.; Choi, J. W. *J. Power Sources*, **2007, 172**: 198

4 Gu, L.; Luo, N.; Miley, G. H. *J. Power Sources*, **2007, 173**: 77

5 Miley, G. H.; Luo, N.; Mather, J.; Burton, R.; Hawkins, G.; Gu, L.; Byrd, E.; Gimlin, R.; Shrestha, P. J.; Benavides, G.; Laystrom, J.; Carroll, D. *J. Power Sources*, **2007, 165**: 509

6 Raman, R. K.; Choudhury, N. A.; Shukla, A. K. *Electrochem. Solid-State Lett.*, **2004, 7**: 488

7 Yang, W.; Yang, S.; Sun, W.; Sun, G.; Xin, Q. *Electrochim. Acta*, **2006, 52**: 9

8 Yang, W.; Yang, S.; Sun, W.; Sun, G.; Xin, Q. *J. Power Sources*, **2006, 160**: 1420

9 Medeiros, M. G.; Bessette, R. R.; Deschenes, C. M.; Patrissi, C. J.; Carreiro, L. G.; Tucker, S. P.; Atwater, D. W. *J. Power Sources*, **2004, 136**: 226

10 Dow, E. G.; Bessette, R. R.; Seeback, G. L.; Marsh-Orndorff, C.; Meunier, H.; Van Zee, J.; Medeiros, M. G. *J. Power Sources*, **1997, 65**: 207

11 Bessette, R. R.; Medeiros, M. G.; Patrissi, C. J.; Deschenes, C. M.; LaFratta, C. N. *J. Power Sources*, **2001, 96**: 240

12 Bessette, R. R.; Cichon, J. M.; Dischert, D. W.; Dow, E. G. *J. Power Sources*, **1999, 80**: 248

13 Brodrecht, D. J.; Rusek, J. J. *Appl. Energy*, **2003, 74**: 113

14 Hasvold, O.; Johansen, K. H.; Mollestad, O.; Forseth, S.; Storkersen, N. *J. Power Sources*, **1999, 80**: 254

15 Medeiros, M. G.; Dow, E. G. *J. Power Sources*, **1999, 80**: 78

16 Hasvold, O.; Storkersen, N. J.; Forseth, S.; Lian, T. *J. Power Sources*, **2006, 162**: 935

17 Cao, D.; Chao, J.; Sun, L.; Wang, G. *J. Power Sources*, **2008, 179**: 87

18 Cao, D.; Sun, L.; Wang, G.; Lv, Y.; Zhang, M. *J. Electroanal. Chem.*, **2008, 621**: 31

19 Luo, N.; Miley, G. H.; Shrestha, P. J.; Gimlin, R.; Burton, R.; Hawkins, G.; Mather, J.; Rusek, J.; Holcomb, F. In Proceeding of Eighth International Hydrogen Peroxide Propulsion Conference, Purdue University, Lafayette, IN, USA, 2005, September 18–21, 2005: 87–96

20 Medeiros, M. G.; Bessette, R. R.; Deschenes, C. M.; Atwater, D. W. *J. Power Sources*, **2001, 96**: 236

21 Liu, H.; Zhang, L.; Zhang, J.; Ghosh, D.; Jung, J.; Downing, B. W.; Whittemore, E. *J. Power Sources*, **2006, 161**: 743

22 Dias, V. L. N.; Fernandes, E. N.; da Silva, L. M. S.; Marques, E. P.; Zhang, J.; Marques, A. L. B. *J. Power Sources*, **2005, 142**: 10

23 Raman, R. K.; Shukla, A. K. *J. Appl. Electrochem.*, **2005, 35**: 1157

24 Ravindra, N. S.; Koenig, J. F.; Poillerat, G.; Chartier, P. *J. Electrochem. Soc.*, **1990, 137**: 1408

25 Rashkova, V.; Kitova, S.; Konstantinov, I.; Vitanov, T. *Electrochim. Acta*, **2002, 47**: 1555

26 Wu, G.; Li, N.; Zhou, D. R.; Mitsuo, K.; Xu, B. Q. *J. Solid State Chem.*, **2004, 177**: 3682

27 Singh, R. N.; Koenig, J. F.; Poillerat, G.; Chartier, P. *J. Electroanal. Chem.*, **1991, 314**: 241

28 Marco, J. F.; Gancedo, J. R.; Gracia, M.; Gautier, J. L.; Rios, E.; Berry, F. J. *J. Solid State Chem.*, **2000, 153**: 74

29 Kim, J. G.; Pugmire, D. L.; Battaglia, D.; Langell, M. A. *Appl. Surf. Sci.*, **2000, 165**: 70

30 De Faria, L. A.; Prestat, M.; Koenig, J. F.; Chartier, P.; Trasatti, S. *Electrochim. Acta*, **1998, 44**: 1481

31 Van Venrooij, T. G. J.; Koper, M. T. M. *Electrochim. Acta*, **1995, 40**: 1689

32 Matsumoto, F.; Uesugi, S.; Koura, N.; Ohsaka, T. *J. Electroanal. Chem.*, **2003, 549**: 71

33 Heller-Ling, N.; Prestat, M.; Gautier, J. L.; Koenig, J. F.; Poillerat, G.; Chartier, P. *Electrochim. Acta*, **1997, 42**: 197

34 Angelo, A. C. D.; Gonzalez, E. R.; Avaca, L. A. *Int. J. Hydrogen Energy*, **1991, 16**: 1

35 Bagotzky, V. S.; Shumilova, N. A.; Khrushcheva, E. I. *Electrochim. Acta*, **1976, 21**: 919